

Evaluation of the Virtual Crystal Approximation for Predicting Thermal Conductivity

Jason M. Larkin¹ and A. J. H. McGaughey^{2,*}

¹*Department of Mechanical Engineering*

Carnegie Mellon University

Pittsburgh, PA 15213

²*Department of Mechanical Engineering*

Carnegie Mellon University

Pittsburgh, PA 15213

(Dated: January 24, 2013)

Abstract

In this work, the virtual crystal approximation for mass disorder is evaluated by examining two model alloy systems: Lennard-Jones argon and Stillinger-Weber silicon. In both cases the perfect crystal is alloyed with a heavier mass species up to equal concentration and phonon properties and thermal conductivity are predicted. These two alloyed systems have different ranges of phonon frequencies, lifetimes, and mean free paths. For Stillinger-Weber silicon, the virtual crystal approximation predicts phonon properties and thermal conductivity in good agreement with molecular dynamics-based methods. For Lennard-Jones argon, the virtual crystal approximation underpredicts the high frequency phonon lifetimes, leading to an underpredicting of its thermal conductivity. Resolution of these underpredictions is achieved by considering methods which treat the disorder explicitly.

I. INTRODUCTION

Predicting the thermal conductivity of disordered lattices dates back to... In the case of semiconductors, almost all of the heat is conducted by the vibrational modes of the system. Understanding the mechanisms that lead to the scattering of these vibrations is crucial for predicting the thermal conductivity of disordered lattices.

To improve the efficiency of thermoelectric devices, efforts to reduce thermal conductivity using several techniques, including micro- and nano-boundary scattering. These techniques often require complicated nanostructuring and manufacturing techniques. Alloying remains an effective method to reduce the thermal conductivity of materials. In particular, for materials with short phonon mean free path spectra, alloying is still a potential thermal conductivity reduction mechanism where nanostructuring is not.¹

Accurately predicting the thermal conductivity of a dielectric or semiconducting material requires the properties of phonons from the entire Brillouin zone. Accurate predictions of phonon properties for bulk systems can be made with anharmonic lattice dynamics (ALD) theory using ab initio calculations.¹⁻⁷ However, computational costs limit the size of computational cells in ab initio calculations to be less than 100 atoms, making it difficult to directly incorporate the effects of disorder.^{1,3,4,8,9}

Recently, work using ab-initio calculations, anharmonic lattice dynamics (ALD) and the virtual crystal (VC) approximation was done to predict phonon mode frequencies, lifetimes and group velocities of defected materials with relatively large^{3,4} and small¹ thermal conductivities. Under this approximation, the disordered crystal is replaced with a perfect virtual crystal with properties equivalent to an averaging over the disorder (e.g. mass or bond strength).¹⁰ The use of ALD with VC (referred to herein as VC-ALD) bases all calculations on a small unit cell with averaged properties and treats the effects of intrinsic and disorder scattering as perturbations rather than including disorder explicitly.^{1,3,10,11} However, no comprehensive study has been performed to assess the applicability of this perturbative approach for a range of disorder using multiple predictive methods and test systems.

The goal of this work is to investigate the use of the VC approximation for predicting thermal conductivity of disordered lattices by a detailed comparison of 3 predictive methods: MD-based normal mode decomposition (NMD, Section) and green-kubo (GK, Section ??), and VC-ALD which treats the harmonic and anharmonic phonon scattering as perturbations

(Section IF 2). Two model binary-alloy systems (labeled as $m_{1-c}^a m_c^b$, Section) with varying concentrations (c) of mass defects are considered: Lennard-Jones (LJ) argon and Stillinger-Weber (SW) silicon. In both cases the perfect crystal is alloyed with a heavier mass species up to equal concentration ($c = 0.5$), spanning a range of perturbative to heavy disorder. By spanning this range, the limits of the perturbative models are examined.

The LJ argon and SW silicon alloyed systems have very different ranges of phonon frequencies, lifetimes, group velocities and total thermal conductivity. For SW silicon, VC-ALD predicts thermal conductivity in good agreement with the explicitly disordered method GK (Section). For LJ argon, VC-ALD underpredicts the high frequency phonon lifetimes, leading to an underpredicting of the thermal conductivity when compared to the explicitly disordered methods VC-NMD and GK (Section). The different thermal conductivity spectra and the breakdown of the perturbative models are examined. Resolution of the breakdown is achieved by including the explicit effect of disorder on the thermal transport of vibrational modes (Section). Based on the effects of explicit disorder, a simple guideline is suggested for use with the VC approximation.

not used yet... Experimental measurements of isotopically pure and Ge-doped Si epitaxial layers demonstrate the original theory by Abeles can predict thermal conductivity in dilute alloys. Abeles also found good agreement with dilute predictions for both experimental measurements of both Si-Ge alloys and also (Ga,In)As alloys.¹⁰ However, both of these alloy systems have a relatively high thermal conductivities (on the order of 1-10 W/m-K at 300 K). However, in the heavily disordered system In(As,P) (mass ratio of 3.7) worse agreement with the Abeles theory is observed.

A. Virtual Crystal (VC) Approximation

Abeles first introduced the idea of using a virtual crystal (VC) to replace a disordered one, computing the thermal conductivity of Si/Ge alloys by treating both disorder and anharmonicity as perturbations.¹⁰ Many experimental trends in thermal conductivity of a range of materials can be explained using the VC approximation.(cite) For example, the reduced thermal conductivity of Ge versus Si is partly explained by both the increased mass and decreased bulk modulus (stiffness) of the lattice,(cite) which has the effect of reducing the phonon group velocities. The same effect can be seen in alloy systems.(cite) Sound

speeds of alloys: CRC, (Cahill-Pohl).

A complete description of the thermal transpot in both perfect crystals and alloys requires modeling the intrinsic and disordered scattering to calculate phonon lifetimes (see Section IF 2). Phonon lifetimes can be predicted by treating both the intrinsic and disorder scattering using perturbation theory (Section). While the theory which treats phonon defect scattering (Eq.) is valid for perturbative disorder, its use leads to good agreement with several experimental and computational results with large disorder. Cahill shows that conductivity reduction in dilute Ge-doped Si epitaxial layers is captured by mass perturbative disorder.^{12,13} While the mass disorder was large ($m_{Ge}/m_{Si} = 2.6$), the overall disorder strength is dictated by the concentration. As little as $6.2 \times 10^{19} cm^{-3}$ Ge ($g_2 = 3.1 \times 10^{-3}$, see Section) is enough to reduce the thermal conductivity of Si by almost a factor of 2.¹² Even in the case of $Ni_{0.55}Pd_{0.45}$, with large mass disorder and concentration ($m_{Pd}/m_{Ni} \approx 2$, $g_2 = 0.078$ Section), good agreement is also seen using a VC approach.¹⁴ What is thermal conductivity of NiPd alloy versus amorphous phase, what is the HS prediction.

Computational results using the VC approximation for high thermal conductivity alloys show good to excellent agreement with experimental results^{3,4}. Garg used ab initio calculations with VC-ALD to predict the thermal conductivity of Si/Ge alloys for all concentrations, obtaining excellent agreement with experiment.⁴ Does Garg find factor of 2 change for intrinsic lifetimes, or the combination of intrinsic and defect with Matthiesen rule? Lindsay and Broido found good agreement with VC-ALD and experiment for isotopically defected GaN.³ Isotopically defected GaN and Si/Ge alloys (even for large concentrations c , Section) have relatively large thermal conductivities.(cite) In particular, the conductivity of Si/Ge alloys is significantly larger than that of the high scatter limit (Section). A detailed study of low thermal conductivity materials PbTe⁵ and PbTe/PbSe¹ made predictions for the perfect systems in fair agreement with experiment, where results lack for the alloys. What is the PbTe HS prediction. Thus, there is a need to examine the perturbative approach of VC-ALD for heavily disordered systems. The computational studies discussed above were limited to the use of VC-ALD because of the computational cost of ab initio calcualtions. Computationally cheap empirical potentials can be used to incude the effects of disorder explicitly.

Using computationally-cheap empirical potentials for argon and silicon¹⁵, we study the effects of disorder explicitly. Using the VC approximation, we perform calculations at dif-

ferent concentrations (c) of mass varying ($m_{1-c}^a m_c^b$) binary alloys of Lennard-Jones argon and Stillinger-Weber silicon (Section). We predict the phonon mode properties of the VC: frequencies (Section), group velocities (Section), and lifetimes (Section), and use them to predict thermal conductivity (Section). Methods referred to as VC-NMD (Section) and VC-ALD (Section) use the VC approximation. Explicit disorder is examined using lattice dynamics (LD) calculations (Section and), Allen-Feldman theory (Section),¹⁶ and molecular dynamics (MD) simulations (Section). The breakdown of the perturbative VC-ALD method is examined (Section), and a simple correction is suggested by predictions from the AF theory (Section).

dunno where this belongs.

While the group velocities are necessary to predict the thermal conductivity, of particular interest is the phonon mean free path (MFP),

$$\Lambda(\kappa) = |\mathbf{v}_g| \tau(\kappa), \quad (1)$$

which is crucial for understanding nano and micro-nanostructuring effects.(cite) It is correct to regard the mode lifetime $\tau(\kappa)$ as the more fundamental quantity in a disordered system,(cite) since there is no general way to predict the group velocities of disordered modes.(cite) The effect of disorder on mode group velocities is examined in (Section) and (Section).

B. Thermal Conductivity Models

To predict the thermal conductivity of disordered lattices, one begins with the theory for a perfect lattice. For a perfect lattice, all vibrational modes are phonons, which by definition are delocalized, propagating plane waves.(cite) Using the single-mode relaxation time approximation¹⁸ as an approximate solution of the Boltzmann transport equation¹⁹ gives an expression for thermal conductivity,

$$k_{ph,\mathbf{n}} = \sum_{\kappa} \sum_{\nu} c_{ph}(\kappa) \mathbf{v}_{g,\mathbf{n}}^2(\kappa) \tau(\kappa). \quad (2)$$

Here, the phonon mode has frequency $\omega(\kappa)$ (Section), c_{ph} is the phonon volumetric specific heat, $v_{g,\mathbf{n}}$ is the component of the group velocity vector in direction \mathbf{n} (Section), and $\tau(\kappa)$ is the phonon lifetime (Section). The SMRT approximation has been shown to be accurate for

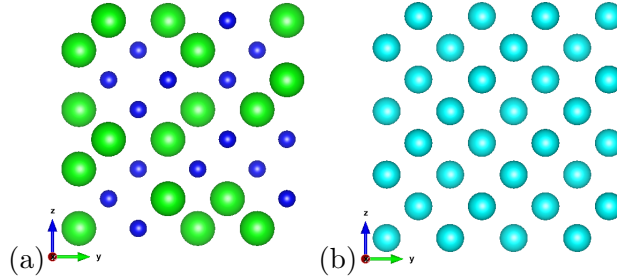


FIG. 1: (a) view of an explicitly disordered supercell of Si and “heavy” Si ([100] direction into the paper).¹⁷ (b) view of the equivalent VC supercell with an average mass of the explicitly disordered Si and “heavy” Si supercell (b). Sphere size represents increasing mass only, no bond disorder is considered. In this work, calculations for LJ Ar and SW Si which use the VC approximation are based off of the conventional cubic unit cells (Section ID, ??, IF 1 and IF 2). The explicitly disordered supercells are used in Sections ID, IE 2, IF 1 and ??.

Si/Ge systems and lower thermal conductivity materials, while larger conductivity materials such as GaN and Diamond require a full iterative solution to the BTE for more accurate results.²

For the perfect cubic lattices considered in this work (see Section), the lattices and the components of their thermal conductivity are cubically symmetric, so that we refer to k_{ph} only. This is also true for the disordered lattices in the long wavelength limit. Since the MD simulations we perform (Section) are classical and obey Maxwell-Boltzmann statistics,²⁰ the specific heat is k_B/V per mode in the harmonic limit, where V is the system volume. This approximation has been shown to be valid for LJ Ar(cite SED or ASME?) and SW Si(cite SED or ASME?) and is used for all calculations in this work so that direct comparisons can be made for all methods.

In the classical-harmonic limit, the thermal conductivity is determined by the thermal diffusivity of each mode, which for phonons is the product of the group velocity and lifetime (see Section). For the perturbative VC-ALD models (Section), the group velocities are calculated from the dispersion curves and the lifetimes computed by Eq without the use of explicit disorder. For VC-NMD, the group velocities are calculated from the dispersion curves and the lifetimes predicted from MD simulation with explicit disorder (Section).

For explicitly disordered systems, the Allen-Feldman (AF) theory computes the contrib-

bution of diffuson modes to vibrational conductivity (Section) and was developed to predict the thermal conductivity of a-Si.¹⁶ In the AF theory, the thermal conductivity is written as

$$k_{AF} = \sum_{\omega} \frac{k_B}{V} D_{AF}(\omega(\boldsymbol{\nu})), \quad (3)$$

where D_{AF} is the mode-specific thermal diffusivity of disordered vibrational modes defined at the wavevector [000] (referred to as Gamma, Section). The relative contribution of both phonons and diffusons to the total vibrational conductivity, $k_{vib} = k_{ph} + k_{AF}$, has been estimated for a-Si.²¹ While studies have been performed on alloying the amorphous phase, the AF theory has not been applied to disordered lattices.²² In the current study of disordered lattices, the AF theory predictions help to provide a lower limit for the contribution of a given vibrational mode to thermal transport within the computational framework of the VC approximation (Section). This is essential given the computational cost of the AF theory (Appendix), and is also convienient given the simplicity of the VC computational framework.

C. Simulation Details

Perfect and explicitly disordered lattice supercells are generated with atomic positions based on LJ argon’s FCC ($n = 4$) and silicon’s diamond-FCC ($n = 8$) crystal structure, where n is the number of atoms in the unit cell.(cite) Supercells are built cubically with size N_0 , where N_0 refers to the number of repetitions of the unit cell in all 3 spatial directions. Supercells up to size $N_0 \leq 12$ for LJ argon (6096 atoms) are used for calculations. For SW silicon, $N_0 \leq 10$ (SW silicon, 8000 atoms) are used for the MD-based methods, and $N_0 \leq 38$ for VC-ALD (see Appendix D).

Disorder is created by randomly specifying the masses of the atoms on the lattice. The composition of the lattices is labeled by $m_{1-c}^a m_c^b$, where $m^a = 1$ and $m^b = 3$ in LJ units for argon and $m^a = m_{Si}$ and $m^b = 2.6m_{Si}$ for SW silicon and “heavy silicon” (mass of germanium). For $c = 0.5$, the LJ VC has average mass of 2. The supercells are built using the zero-pressure finite-temperature lattice constants for LJ argon, which are $a = 1.556$ (T=10 K) and $a = 1.580$ (T=40 K) in LJ units.²³ For LJ argon, the variation of lattice constant with composition is small and ignored. The effective zero-pressure lattice constant of the amorphous phase at T=10K is slightly larger ($a = 1.585$).²³ All LJ calculations

use these lattice constants. For SW silicon, the lattice constant $a = 5.43\text{\AA}$ is used for all calculations, which brings the GK thermal conductivity predictions²⁴ into better agreement with VC-ALD²⁵ for $c = 0.0$ (Section).

D. VC and Gamma DOS

In this section, we examine the effect of explicit disorder by computing the density of states (DOS, $D(\omega(\kappa))$) for vibrational modes of and of the disordered lattice supercells and their equivalent VCs. Each vibrational mode contributing to the thermal conductivity has a frequency $\omega(\kappa)$. The allowed frequencies are the square root of the eigenvalues of the system's Dynamical matrix, $D(\kappa)$,²⁶ which relates the normal mode eigenvector ($e(\kappa)$) and eigenvalue by

$$D(\kappa)e(\kappa) = \omega^2(\kappa) e(\kappa). \quad (4)$$

The set of eigenvalues and eigenvectors are the orthonormal basis of the vibrational lattice.²⁶ In a perfect system all vibrational (normal) modes are plane-waves, and as such can be identified by a wave-vector κ , eigenvector $e(\kappa)_\alpha^b$, and a possibly degenerate frequency $\omega(\kappa)$. Here, b labels the atom in the unit cell, α labels the cartesian coordinates, and ν labels the mode polarization (possibly degenerate in frequency). In a disordered system, such as a lattice supercell with randomly arranged and differing mass species, all normal modes exist at the wavevector [000], where $n = N_a$ and $\nu \leq 3N_a$, where N_a is the total number of atoms in the system. However, for small disorder ($c \approx 0$), the modes of the disordered lattice are nearly plane-waves. In general, normal modes in a disordered system will not be pure plane-waves and will be non-degenerate in frequency. We compare the ordered and disordered normal mode frequencies in Section ?? and mode eigenvectors in Section for the full range of disorder ($c \leq 0.5$).

With the appropriate dynamical matrix ($\kappa = [000]$ for the explicitly disordered lattice supercells), the frequencies are computed using the program GULP.²⁷ For the VC, the frequencies are identified (up to polarization) by the list of wavevectors allowed by the size of the lattice supercell.(cite) The DOS for the VC and the explicitly disordered supercells (referred to herein as Gamma) are shown in Fig. . The VC and Gamma agree at low frequencies, where the Debye approximation predicts $DOS(\omega) \propto \omega^2$.(cite) The Debye approximation underpredicts the the DOS at moderate frequency, which is due to the non-linear

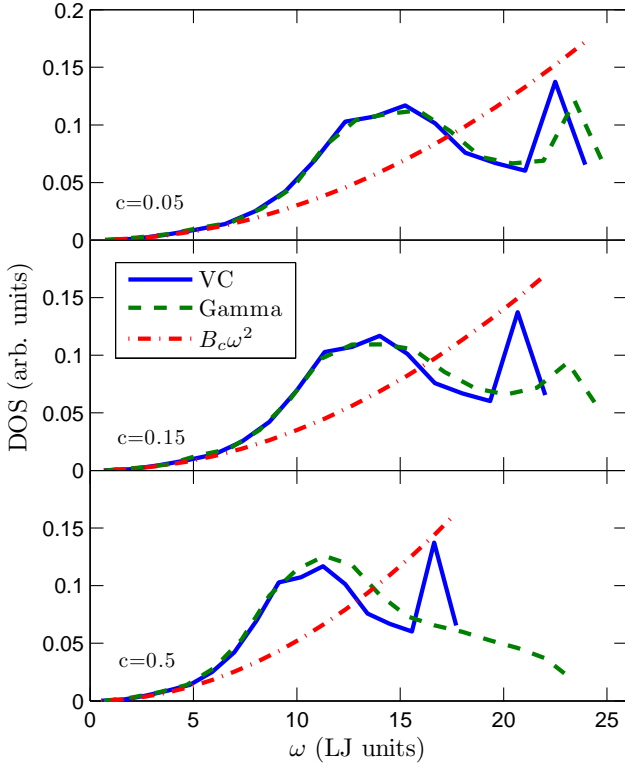


FIG. 2: Density of states (DOS) for modes calculated using the LJ FCC VC versus an explicitly mass disordered LJ FCC supercell (labeled Gamma) with varying mass concentration c (Section). VC and Gamma show similar low frequency behavior for all c . For increasing c , the frequencies of both VC and Gamma decrease, while the high frequency DOS for Gamma spreads and reaches up to a higher maximum frequency because of the explicit disorder. The size of these supercells is $N_0 = 12$ (see Section).

dispersion.(cite Mermin)

The increasing lattice mass with increasing c for the VC has the effect of reducing the frequencies. The increasing lattice mass for the Gamma modes also has the effect of reducing the frequencies. However, the effect of explicit disorder can be seen at high frequencies by a broadening and a shift of the DOS to higher frequencies because of the explicit use of light atoms in the supercell. Duda et al observed similar high-frequency broadening effects in model LJ alloys.²⁸ Similar agreement at low frequencies was found in ab initio predictions for Si_cGe_{1-c} ,⁴ while Bouchard showed similar continuous behavior at low frequency for a- Si_cGe_{1-c} .²⁹

E. Dispersion

1. From VC

The group velocity vector in a VC is the gradient of the dispersion curves,

$$v_{g,n}(\kappa) = \partial\omega(\kappa)/\partial\kappa, \quad (5)$$

which can be calculated from the frequencies and wavevectors using finite differences. In this work, the group velocities for the VC are calculated using finite difference and quasi-harmonic lattice dynamics.³⁰

In general, real systems have dispersion which depends on the wavevector and polarization. For simple systems, such as LJ argon, the dispersion has only 3 polarizations ν , 1 longitudinal and 2 transverse acoustic branches.²⁶ For SW silicon, the 2-atom basis creates optical modes which have distinctly different dispersions than acoustic branches, and hence have different group velocities. For systems with a large basis or low-symmetry, the dispersion can be very complicated.(cite)

Except for the three acoustic branches (2 transverse, 1 longitudinal), there is not an accepted method to predict the effective group velocity of a vibrational mode in a disordered system, though there are attempts.^{21,28,31–33} In the Cahill-Pohl (CP) model, the group velocity of all disordered modes is the sound speed v_s (Section).³¹ Dispersion for a model disordered 1D system attributes the reduction of group velocities due to a zone-folding effect.²⁸ In studies of disordered silicon systems, the group velocity of vibrational modes was estimated using an interpolation scheme for small but finite wavevectors near [000].^{21,32,33} footnote (We do not, in general, observe the required dispersion behavior near the Gamma point to perform the interpolation for the LJ and SW systems studied in this work.^{21,32,33})

Feldman et al used the structure factor to predict an effective dispersion for a model of a-Si, but did not predict group velocities.³⁴ Volz and Chen used the dynamic structure factor to predict the dispersion of SW Si using MD simulation, which is a perfect system.³⁵ As a method to predict mode group velocities, we examine the structure factor for the explicitly disordered modes in the next section.

2. From Structure Factor of Gamma Modes

Calculating the structure factor of Gamma modes is a method to test for the plane-wave character of disordered modes at a particular wavevector and polarization.^{34,36} The structure factor is defined as³⁶

$$S^{L,T}(\kappa) = \sum_{\nu} E^{L,T}(\nu) \delta(\omega - \omega(\nu)), \quad (6)$$

where E^T refers to transverse polarization and is defined as

$$E^L(\nu) = \left| \sum_{l,b} \hat{\kappa} \cdot e(\nu^b_{\alpha}) \exp[i\kappa \cdot \mathbf{r}_0(b)] \right|^2 \quad (7)$$

and E^L refers to longitudinal polarization and is defined as

$$E^T(\nu) = \left| \sum_{l,b} \hat{\kappa} \times e(\nu^b_{\alpha}) \exp[i\kappa \cdot \mathbf{r}_0(b)] \right|^2. \quad (8)$$

Here, $\mathbf{r}_0(b)$ refers to the lattice positions in the mass disordered atoms in the supercells, which are still spatially ordered. Explicit disorder is accounted for in the mode frequencies $\omega(\nu)$ and eigenvectors $e(\nu^b_{\alpha})$ which are calculated with $\kappa = [000]$.

Physically, $S^{L,T}(\kappa)$ calculates the frequency spectrum required to create a wavepacket with well-defined wavevector and polarization.^{34,36} The details of the calculation are given in Appendix. For a perfect lattice, the structure factor peaks are delta functions centered at the phonon mode frequencies, indicating they are pure plane-waves. With increasing disorder (c), the structure factor spreads in width, particularly at high frequencies (Fig) because the modes are no longer pure plane-waves. An effective dispersion can be extracted by locating the peaks in the structure factors, where the effects of polarization, virtual mass, and anisotropic dispersion can be observed (Fig.). As the lattice VC mass becomes larger, the peaks in the structure factor shift to lower frequencies. The peaks in the structure factor are shifted to slightly higher frequencies than the VC predicted frequencies by up to only %5. Similar good agreement can be seen with the disordered SW silicon lattices, while the structure factors are more complicated because of the optical modes. Because of this good agreement, we use the group velocities predicted by the VC dispersion for both LJ argon and SW silicon with the VC-NMD and VC-ALD calculations for consistency and simplicity (Section and Appendix C). We examine the validity of this choice of group velocity in Section . Well-defined peaks (see Appendix) at all wavevectors are most likely due to the

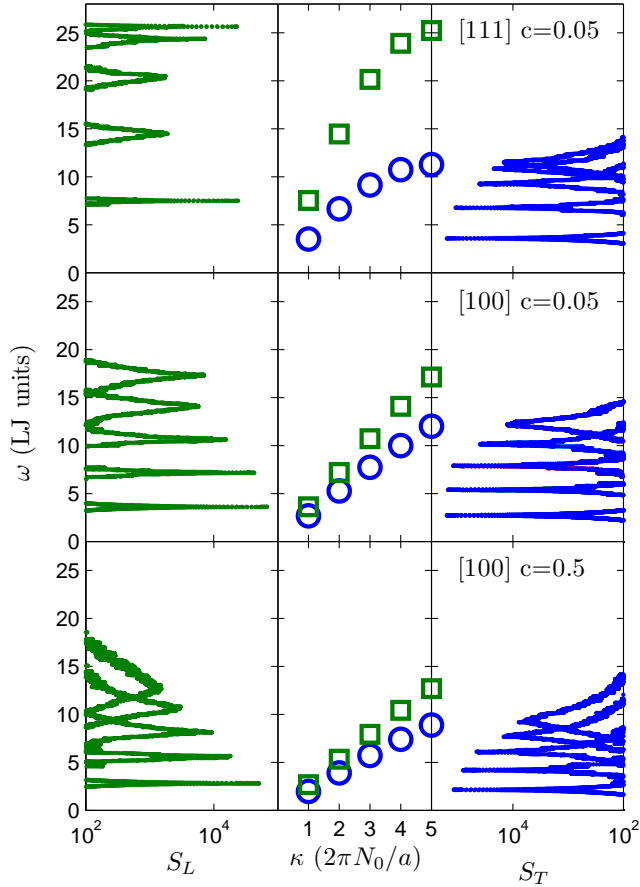


FIG. 3: Left and Right Panels: The structure factor for longitudinal (S_L) and transverse (S_T) polarizations along high symmetry directions ([100], [110] where $\kappa = \pi/a[100]$ and a is the lattice constant) of the mass disordered LJ FCC supercells ($c = 0.05, 0.5$). For increasing mass disorder c , there is a decrease in the center of the peaks and an increase in the peak linewidths. Center Panel: The VC predicted dispersion at the same wavectors used to calculate $S_{L,T}$.

lattice structure of the disordered systems studied in this work. Typically, the structure factor for amorphous materials has well-defined peaks only for small wavevector, which is related to the thermal diffusivity of the disordered modes.^{34,36}

F. Lifetimes

1. From VC-NMD and Gamma

As an alternative to the VC-ALD models for predicting phonon lifetimes (Section), we use the normal mode decomposition (NMD) method.^{37,38} NMD maps the atomic trajectories (positions and velocities) of atoms in an MD simulation onto the vibrational normal mode coordinates,(cite)

$$q(\boldsymbol{\kappa}; t) = \sum_{\alpha,b,l}^{3,n,N} \sqrt{\frac{m_b}{N}} u_\alpha(l; t) e^*(\boldsymbol{\kappa}_\alpha^b) \exp[i\boldsymbol{\kappa} \cdot \mathbf{r}_0(l)] \quad (9)$$

and

$$\dot{q}(\boldsymbol{\kappa}; t) = \sum_{\alpha,b,l}^{3,n,N} \sqrt{\frac{m_b}{N}} \dot{u}_\alpha(l; t) e^*(\boldsymbol{\kappa}_\alpha^b) \exp[i\boldsymbol{\kappa} \cdot \mathbf{r}_0(l)]. \quad (10)$$

where $\mathbf{r}_0(l)$ are the equilibrium positions of the atoms in the l th unit cell of the lattice supercell under the VC approximation. (needs work) The total energy of a given mode is given by

$$E(\boldsymbol{\kappa}; t) = \frac{\omega(\boldsymbol{\kappa})}{2} q(\boldsymbol{\kappa}; t)^* q(\boldsymbol{\kappa}; t) + \frac{1}{2} \dot{q}(\boldsymbol{\kappa}; t)^* \dot{q}(\boldsymbol{\kappa}; t) \quad (11)$$

The MD simulation is performed using the perfect and disordered supercells (Section, Fig.). The NMD is performed using the frequencies and eigenvectors from both the VC ($\omega(\boldsymbol{\kappa})$, $e(\boldsymbol{\kappa}_\alpha^b)$) and the Gamma supercell ($\omega(\boldsymbol{\kappa})$, $e(\boldsymbol{\kappa}_\alpha^b)$ with $\boldsymbol{\kappa} = [000]$, Section). The vibrational mode frequencies and eigenvectors are necessary for the mapping of the atomic trajectories from the MD simulation onto the vibrational normal mode coordinates, $q(\boldsymbol{\kappa}; t)$ and $\dot{q}(\boldsymbol{\kappa}; t)$, which are required to calculate the kinetic, potential, and total ($E(\boldsymbol{\kappa})(t)$) vibrational normal mode energies.(cite) The effects of disorder enter through the trajectories from these MD simulations, which are also used for the GK method (Section).

The normal mode lifetime is predicted using

$$\tau(\boldsymbol{\kappa}) = \int_0^\infty \frac{\langle E(\boldsymbol{\kappa}; t) E(\boldsymbol{\kappa}; 0) \rangle}{\langle E(\boldsymbol{\kappa}; 0) E(\boldsymbol{\kappa}; 0) \rangle} dt, \quad (12)$$

where the indefinite integral is replaced by a finite integration given the specifications of the MD simulation. This method for predicting the mode lifetime is more robust than other

methods for the disordered systems studied in this work (see Appendix B). It does, however, make it more difficult to predict a phonon frequency, so we use the VC predicted frequency for all VC-NMD predictions, which allow for easier comparison to VC-ALD (Section).

The lifetimes predicted using VC-NMD and Gamma-NMD are shown in Fig. First, the range of frequencies of the modes for VC-NMD and Gamma-NMD differ slightly, particularly at high frequency, which is due to the difference in the DOS (Fig.). For small intervals of frequency, there are a wider range of predicted lifetimes for Gamma-NMD. This is because there is no symmetry averaging of the mode properties, which is performed for the modes of VC-NMD given that a VC is assumed.(cite)

Lifetimes predicted by both VC-NMD and Gamma-NMD show scalings with frequency which are predicted by the perturbative methods of VC-ALD (Section), in particular scalings of ω^{-2} , ω^{-4} and even faster scaling due to the DOS behavior (Fig. , Section). What is not predicted by the perturbative VC-ALD methods is the behavior at the highest frequencies, where $\tau \text{ constant}$, which is seen roughly for both VC-NMD and Gamma-NMD, except at $c = 0.5$ for VC-NMD. In general, the lifetimes predicted by both VC-NMD and Gamma-NMD are larger than the Ioffe-Regel (IR) limit,³⁹

$$\tau = 2\pi/\omega. \quad (13)$$

The physical interpretation of the IR limit is that of a mode which scatters in a time less than its oscillation period, which is satisfied for most modes in Fig. At the highest frequencies, the existence of this characteristic (thought not exactly minimum) lifetime for LJ argon is analogous to the minimum mean free path used in a simple models of glasses.⁴⁰ There is, however, no theoretical prediction of this high-frequency behavior.

While it is possible to predict a MFP given the VC predicted group velocities and the lifetimes predicted by VC-NMD, we find that it is not useful to understanding this high-frequency behavior. For the group velocities predicted from the VC dispersion, they generally trend towards 0 as the wavevector is increased to the BZ boundaries. This would predict a MFP of 0, which is not helpful to the current discussion. Furthermore, the concept of a MFP becomes poorly defined the more the system is disordered (e.g. dilute alloys to high concentration and amorphous phases). It is thus more useful to consider the proposed lower-limit of the mode thermal diffusivities, which combine the mode lifetime and effective group velocity, or equivalently, effective MFP (Section).

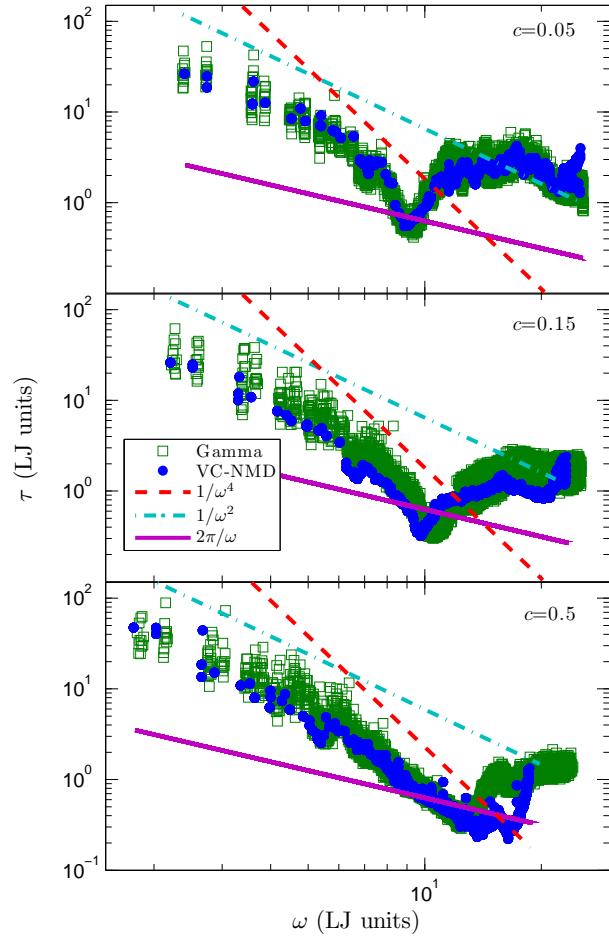


FIG. 4: Lifetimes predicted using VC-NMD and Gamma NMD from MD simulations of mass disordered lattice supercells (Section). Both ω^{-2} and ω^{-4} scalings can be observed at low frequencies, which are predicted by the perturbative models used for VC-ALD (Section). For both VC-NMD and Gamma NMD, most mode lifetimes are greater than the Ioffe-Regel limit $\tau = 2\pi/\omega$.³⁹ While there is more “noise” in the Gamma mode data (Section), the lifetime magnitudes and trends agree well, an important consideration when comparing VC-NMD and VC-ALD in Fig. .

2. From VC-ALD

Assuming intrinsic and disorder scattering mechanisms to operate independently, the effective phonon lifetime can be found using Matthiessen’s rule(cite),

$$\frac{1}{\tau(\nu)} = \frac{1}{\tau_{p-p}(\nu)} + \frac{1}{\tau_d(\nu)}, \quad (14)$$

where $\tau_{p-p}(\kappa_\nu)$ accounts for intrinsic phonon-phonon scattering and $\tau_d(\kappa_\nu)$ accounts for defect scattering.

Phonon-phonon scattering ($\tau_{p-p}(\kappa_\nu)$) is typically treated using anharmonic perturbation theory (ALD) including only 3-phonon processes.^{1,4,38} It has been demonstrated that the effects of higher order n-phonon processes become important at high temperatures (see Section).^{38,41} At low frequencies where the density of states is Debye-like (Section Fig.), $\tau_{p-p}(\kappa_\nu)$ follows a scaling due to both normal ($B_1\omega^{-2}$) and umklapp ($B_2\omega^{-2}$) 3-phonon scattering processes, where the constants B_1 and B_2 are typically fit to experimental data.(cite) The scaling $\tau \omega^{-2}$ can be observed in both the NMD (Fig.) and ALD (Fig.) predicted results.

Using harmonic perturbation theory, Tamura gives a general expression for mass point defect scattering¹¹

$$\frac{1}{\tau_d(\kappa_\nu)} = \frac{\pi}{2N} \omega^2(\kappa_\nu) \sum_{\kappa' \nu'} \delta(\omega(\kappa_\nu) - \omega(\kappa'_\nu')) \sum_b g_2(b) |e^*(\kappa'_\nu b) \cdot e(\kappa_\nu b)|^2, \quad (15)$$

where

$$g_n(b) = \sum_\mu c^\mu(b) (1 - m^\mu(b)/\bar{m}(b))^n, \quad (16)$$

N is the number of unit cells, and c^μ is the concentration, $m^\mu(b)$ is the mass of the μ -th species and \bar{m}^μ is the average mass. For the binary LJ argon and SW silicon alloys considered, there is one atom type in the unit cell with $\mu = a, b$, so that the alloying atom labeled by m_{1-c}^b can be considered to be an “isotope” of atom labeled m_c^a . This convention is appropriate because of the perturbative approach used to derive Eq. , while we consider large disorder up to $c = 0.5$.¹¹

The term $g_2(b)$ is a coupling term which defines the strength of the disorder which depends on the concentration and masses of the different species. (Give values of g for LJ and SW, at all $c =$ they are approimxately the same given the similar mass ratios used, so that the underprediction of VC-ALD for LJ argon is because of the nature of the system.)

needs work above

Bond disorder can be accounted for using a similar expression with an average atomic radius or suitable scattering cross-section.^{42,43} The effect of bond and mass disorder has been investigated computationally by Skye and Schelling for Si/Ge⁴⁴, where it was shown that

mass disorder is the dominant scattering mechanism. In this work we consider only mass disorder.

By considering the symmetry properties of the FCC lattices considered in this work (Section), it can be shown that

$$1/\tau_d(\nu) = \frac{\pi}{2} g_2 \omega^2(\nu) D(\omega(\nu)), \quad (17)$$

where $D(\omega(\nu))$ is the density of states (Section).¹¹ Under the Debye-approximation ($D(\omega(\nu)) \propto \omega(\nu)^2$), the phonon scattering due to mass point-defects is given by $A\omega^{-4}$, where A is a constant related to the unit cell volume, branch-averaged group velocity, and disorder coupling strength ($g_2(b)$ in Eq. above). The frequency dependence (ω^4) is the same as Rayleigh scattering, which is valid at low frequency and observed in both the NMD (Fig.) and ALD (Fig.) predicted results. The disorder scattering scaling is expected to fall off faster than ω^{-4} when $D(\omega(\nu))$ grows faster than the Debye scaling of ω^2 (Fig. , Section). The lifetimes do fall off faster ω^{-4} for the mass disordered LJ FCC supercells for a narrow range of frequencies near $\omega = 10$ in Fig. for $c = 0.05, 0.15$, but seem to follow more closely ω^{-4} for $c = 0.5$.

For the VC-ALD method, the intrinsic $\tau(\nu)_{p-p}$ is calculated using the method described in³⁸, using all classical expressions to remain consistent with the classical MD-based methods NMD and GK (Section). To calculate the disordered lifetimes $\tau(\nu)_d$ (Eq.), it is necessary to broaden the δ function using a Lorentzian function.[1] footnote[1] For all calculations, the Lorentzian was broadened using a value of $100\delta_{\omega,avg}$ (Section). For the system sizes here, the results do not differ significantly if this broadening value is varied manually or by increasing system size (N_0).

Higher-order terms in the Tamura theory can be represented by terms involving g_n (where $b = 1$, Eq. (Eq)) and $I(\omega)$, defined as

$$I(\omega) = \frac{1}{6N} \sum_{(\nu)} \frac{\omega(\nu)^2}{\omega(\nu)^2 - \omega - i\epsilon}, \quad (18)$$

where ϵ is a small number, taken to be $100\delta_{\omega,avg}$. For example, the predicted frequency shifts due to disorder scattering are

$$\delta\omega/\omega = g_2(b) \text{Re}[I(\omega)]/2, \quad (19)$$

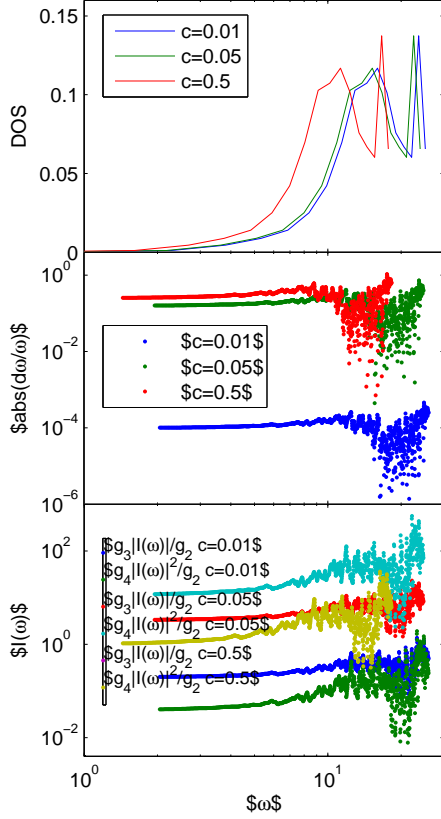


FIG. 5: lj tamura results

and the terms $g_n|I(\omega)|^{n-2}/g_{n-1}$ represent estimates for the higher-order terms of the defect-perturbed phonon self-energy (linewidth), which are shown in Fig (Fig).¹¹ In the original study of isotope scattering in Ge, the perturbation was small and the higher-order terms were shown to be negligible. In the present study, which includes large amounts of disorder (*e.g.* large values of g_n), the predicted frequency shifts and higher-order estimates are not small, especially at high frequency. The effect of these higher-order terms is important to understanding the results predicted by VC-ALD in Section and Section .

G. Diffusivities

In the classical harmonic limit, where the specific heat $c_p(\kappa) = k_B$, a vibrational mode's contribution to thermal conductivity is determined by the mode thermal diffusivity. For phonons, the thermal diffusivity is

$$D_{ph}(\kappa) = \mathbf{v}_g^2(\kappa) \tau(\kappa) . \quad (20)$$

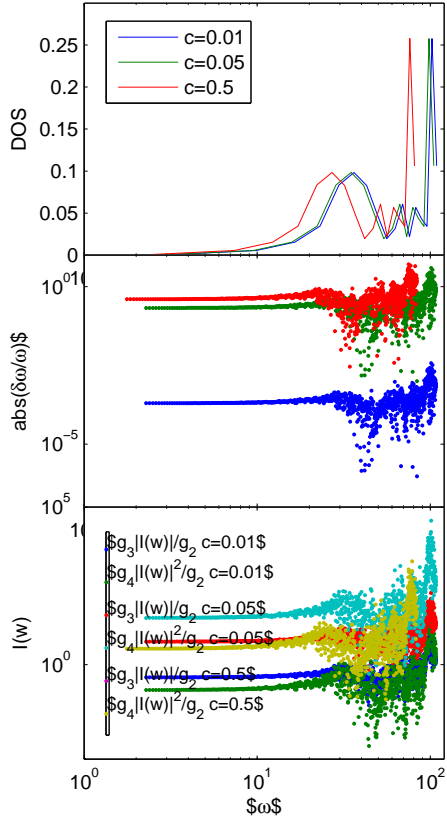


FIG. 6: sw tamura results

Here, $\mathbf{v}_g^2(\kappa)$ is calculated from the VC dispersion (Section) for both VC-NMD and VC-ALD, so any differences in thermal diffusivity comes from the difference in the lifetimes predicted by these two methods.

In explicitly disordered systems, modes can transport heat by harmonic coupling due to disorder in the Allen-Feldman (AF) theory of diffusons.¹⁶ The AF theory predicts the mode-specific thermal diffusivity of disordered vibrations. In the AF theory, the mode diffusivities typically diverges as $\omega - \omega_0 > 0$ because the vibrational modes are long-wavelength plane waves (phonons) that weakly scattered by the disorder.^{45,46} footnote[] (For the disordered lattices studied in this work for $c \leq 0.15$, the predicted k_{AF} is strongly system size dependent, indicating this diverging behavior. For $c = 0.5$, the divergence with system size is small for the range of system size studied ($N_0 = 4$ to $N_0 = 12$), where $k_{AF}/k_{GK} = 0.93$ for $N_0 = 12$.)

In the high-scatter (HS) limit,(cite) the AF diffusivity of each mode is

$$D_{AF,HS} = \frac{1}{3} v_s a, \quad (21)$$

and the AF thermal conductivity prediction in the HS limit is

$$k_{AF,HS} = \frac{k_B}{V_b} b v_s a, \quad (22)$$

where V_b is the volume of the unit cell, v_s is the branch-averaged sound speed, and a is the lattice constant (or appropriate length scale, although the choice of this length scale is not unique).³¹ A similar HS limit for mode diffusivity is given by the Cahill-Pohl (CP) HS model,(cite) $D_{CP,HS} = 0.403v_s a$, which differs from the AF,HS model by a factor of approximately %20.³¹ Ignoring the small difference between the AF,HS and CP,HS models, the physical interpretation is of all vibrational modes with a group velocity equal to the sound speed and mean-free path equal to the lattice spacing. While the CP,HS and AF,HS models assume a constant thermal diffusivity for all modes, the AF theory is capable of predicting the mode specific diffusivities without any assumptions other than a harmonic approximation.(cite)

With sufficient disorder, such as amorphous phases, the harmonic AF theory is capable of accurately predicting a finite thermal conductivity.^{22,47} The thermal conductivity of the LJ amorphous phase (with an effective mass of 2) is predicted by the AF theory, $k_{AF} = 0.099W/m = K$. footnote[] (The amorphous LJ phase was created by liquifying the crystal and instantly quenching by removing all kinetic energy. The resulting structure was then energy minimized and annealed in an NPT ensemble at zero pressure and $T = 10$ K.(cite lammps)) The mode-specific thermal diffusivities for the LJ argon amorphous phase are shown in Fig. , where modes with significant contribution to thermal transport can be modeled using a mode-independent diffusivity of approximately $D_{AF,HS}$ (Eq.). Also shown are the AF predicted thermal diffusivities for the explicitly disordered superlattice and $c = 0.5$.

While the AF theory is divergent in the low-frequency limit for lattices, the finite system size bounds the thermal diffusivities of the lowest frequencies (Fig), and the thermal conductivity predicted by the AF theory is actually quite close to that predicted by the GK method, $k_{AF}/k_{GK} = 0.93$. More importantly, the thermal diffusivity of all modes in the explicitly disordered lattice supercell are finite, except at the highest frequencies where they tend to 0 as in the amorphous phase (Fig). This places a plausible lower-bound on the value of the VC phonon mode diffusivities, $D_{ph} \geq D_{AF,HS}$. In fact, the thermal properties of disordered lattices and glasses has been explained heuristically by assuming that phonons

are scattered so strongly by structural disorder that transport becomes diffusive, with a frequency regime of small, constant thermal diffusivity.^{48,49}

The lower-limit of the thermal diffusivity predicted for the VC modes is $D_{ph}(\kappa_\nu) \approx 0$, as is the case for the VC mode MFP because of the VC predicted group velocities (Section). In typical explicitly disordered system, this lower limit of the thermal diffusivity is only seen for a minority of modes at the highest frequencies, which is true for the disordered LJ systems shown in Fig. Feldman et al showed that the thermal diffusivities in a-Si show a sharp breakpoint at the on-set of localized states, where it tends to zero exponentially. Similar behavior is seen for the LJ argon disordered superlattices and amorphous phase ($c = 0.5$, Fig.).

For both VC-NMD and VC-ALD, a significant number of modes have $D_{ph}(l; t) D_{AF,HS}$ (Fig.). This can lead to an underprediction of the total thermal conductivity. The diffusivity of these modes can be adjusted such that any mode with $D_{ph}(l; t) D_{AF,HS}$ is given $D_{ph} = D_{AF,HS}$. The result of this adjustment, referred to as VC-NMD* and VC-ALD*, is examined in the thermal conductivity predictions in Section .

For LJ argon, VC-NMD predicts lifetimes which are generally larger than the period ($\tau(\kappa_\nu) > 2\pi/\omega(\kappa_\nu)$) of the vibrational oscillation (Ioffe-Regel limit)(cite), and actually increase then remain approximately constant at high frequency (Section and Fig.). VC-ALD predicts essentially monotonically decreasing lifetimes with increasing frequency for both LJ argon and SW silicon (Fig.). Because VC-NMD and VC-ALD use the same values for $v_g(\kappa_\nu)$, the phonon mode diffusivities $D_{ph}(\kappa_\nu)$ are also underpredicted for VC-ALD compared to VC-NMD. There are thus 2 underpredictions to consider when predicting the thermal conductivities in Section : underprediction of the thermal diffusivity assuming the VC phonon modes for VC-NMD and VC-ALD, and the underprediction of the mode lifetimes by the VC-ALD perturbative models.

not used, yet...

energy transport in jammed sphere packings⁵⁰ heat transport in model jammed solids⁴⁶

II. THERMAL CONDUCTIVITY PREDICTIONS

The thermal conductivity can be predicted using the mode properties predicted by the VC-NMD and VC-ALD methods. However, given the discussion of the mode properties

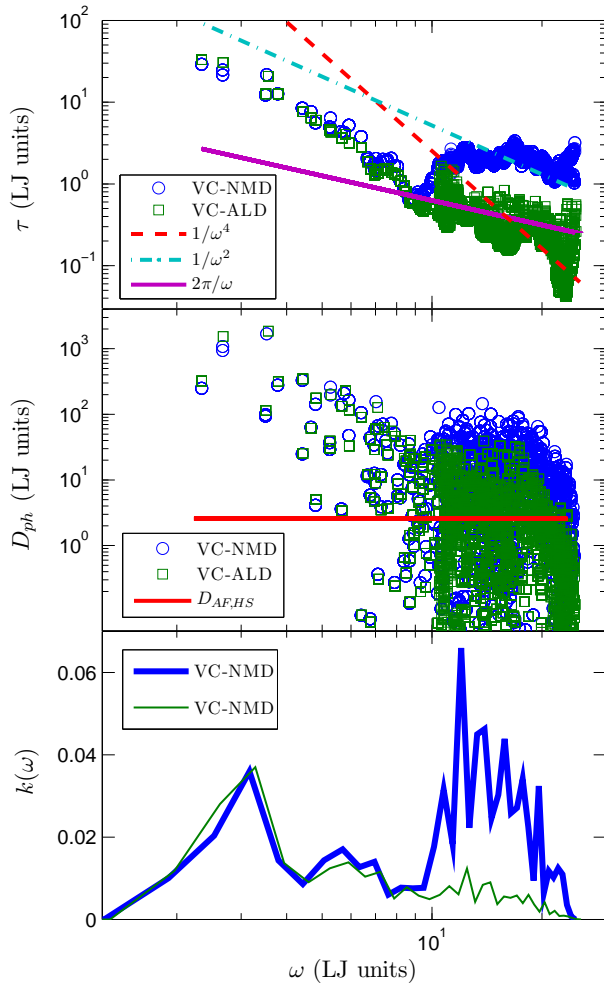


FIG. 7: (a) predicted lifetimes for VC modes using VC-NMD and VC-ALD for LJ argon. (b) predicted VC mode thermal diffusivities, compared to the AF,HS limit. (c) the thermal conductivity frequency spectrum, which is peaked at high frequency, in contrast to SW silicon (Fig).

preceding this section, it is necessary to implement a third method for predicting thermal conductivity. We choose the equilibrium MD-based green-kubo (GK) method. This method does not predict any mode-specific properties, and is thus a system-level prediction. For this reason, thermal conductivity predicted by GK has been shown to capture the effects of whatever scattering mechanisms are present in the MD simulation without any other assumptions (other than those which come with the classical nature of the MD simulation).(cite) Details of the GK and MD simulations are given in Appendix.

For LJ argon, bulk thermal conductivity predictions are made for VC-NMD, VC-ALD

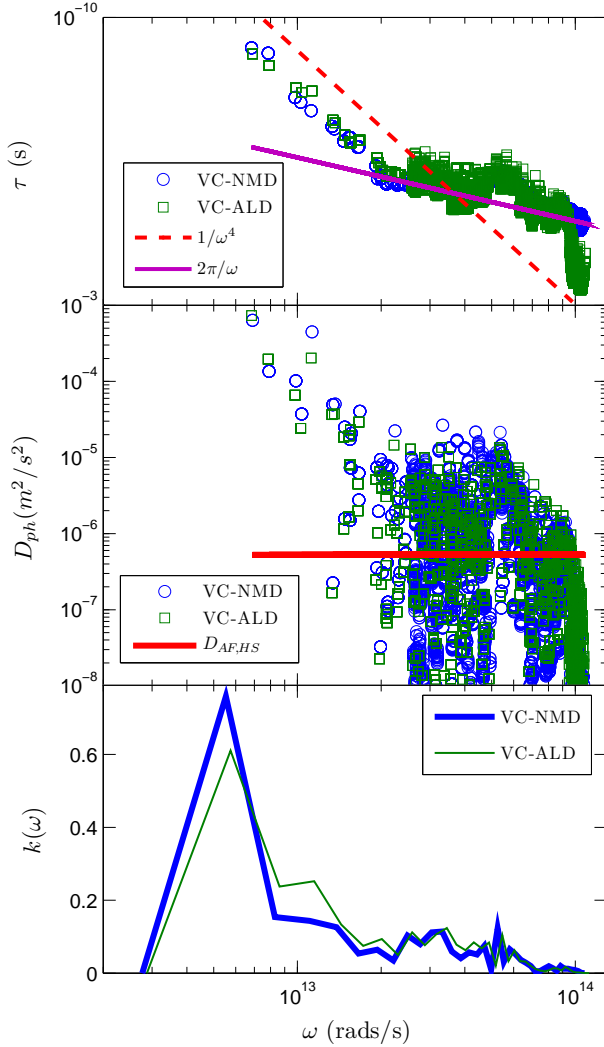


FIG. 8: (a) predicted lifetimes for VC modes using VC-NMD and VC-ALD for SW silicon. (b) predicted VC mode thermal diffusivities, compared to the AF,HS limit. (c) the thermal conductivity frequency spectrum, which is peaked at low frequency, in contrast to LJ argon (Fig).

and GK (Fig.). For SW silicon, bulk thermal conductivity predictions can only be made for VC-ALD and GK because of the limited system size used for VC-NMD (see Appendix). For LJ argon, both VC-NMD and VC-ALD underpredict the thermal conductivity compared to GK.

From Fig. it is clear that both VC-NMD and VC-ALD underpredict compared to GK. The underprediction is only modest for VC-NMD, on the order of 20% or less for all c . By adjusting the mode diffusivity as suggested in Section , the thermal conductivity predicted by VC-NMD* is brought into agreement with GK by approximately 10% or less for all c .

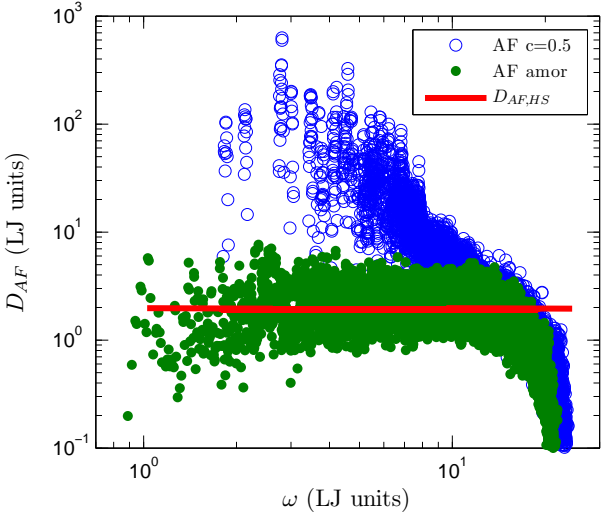


FIG. 9: AF theory predictions of disorded mode thermal diffusivities for LJ argon disorded lattice supercell and amorphous phase. The mode thermal diffusivities predicted for the disorded lattice supercell are all finite, except at the highest frequency where they tend to 0 as in the amorphous phase.

When combined with the high-scatter limit, this suggests that the mode properties predicted by VC-NMD are a fair representation of the explicitly disorderd modes used in the MD simulation.

The VC-ALD method underpredicts the thermal conductivity for all c , where the underprediction is worst at $c = 0.5$ where $k_{VC-ALD}/k_{GK} = 0.56$ and is well outside the error bars of the calculations (which are on the order of the large symbol sizes in Fig.). By applying the high-scatter limit adjustment VC-ALD*, the thermal conductivities are brought into marginally better agreement, worst for $c = 0.05$ where $k_{VC-ALD^*}/k_{GK} = 0.65$. This is because of the underprediction of the mode lifetimes at high frequency for VC-ALD compared to VC-NMD in Section , since the two methods share the same mode group velocities.

The failure of the VC-ALD method can be demonstrated further by moving to higher temerpature ($T = 40$ K Fig.). The beginning breakdown of the intrinsic scattering model ($\tau_{p-p}(\kappa)$) can be observed for the perfect ($c = 0.0$) crystal at $T = 40$ K (see Fig.), where ALD begins to overpredict compared to GK. This can be explained by the emerging importance of higher order ($n > 3$) n-phonon process at high temperatures.³⁸ While the VC-ALD method begins to overpredict at this elevated temperature, it continues to underpredict for the alloys

$c \geq 0.05$. In fact, the thermal conductivity predicted by VC-ALD is right at (and slightly below) the HS limit. This demonstrates that the VC-ALD method is failing to accurately predict the high frequency mode lifetimes similar to $T = 10$ K. The thermal diffusivity adjusted VC-ALD*, again, is only marginally improved.

Because the mode lifetimes are underpredicted at high frequencies for VC-ALD compared to VC-NMD, this leads to an underprediction for VC-ALD of both the thermal conductivity spectrum (Fig.) at high frequency and the total thermal conductivity (Fig.) compared to VC-NMD and GK (Section). As noted in Section , for LJ argon in the amorphous phase, $k_{GK} = 0.121$ W/m-K and $k_{CP,HS} = 0.12$ W/m-K, indicating that almost all important modes to thermal transport are high-scattering. The GK predicted thermal conductivity predictions for the disordered lattices demonstrate that there are important contributions from propagating modes, even at higher temperatures where $k_{GK} > k_{AF,HS}$.

For SW silicon, the thermal conductivities prediction by VC-ALD and GK are in good agreement, even without the adjustment VC-ALD*, which only increases the result from VC-ALD by about 1%. In SW silicon, even the amorphous phase has significant contributions from propagating modes which are considered to be phonons.(cite) Without any detailed mode-by-mode analysis, comparing the thermal conductivity predicted for the SW silicon amorphous phase ($k_{GK} \approx 3$ W/m-K (cite)) compared to the HS limit, $k_{AF,HS} = 0.5$ W/m-K, demonstrates that there is significant contribution from what can be considered propagating modes.(cite) In fact, for a-Si, the mode diffusivities vary as a function of frequency,^{22,34,36} which has been used to explain the propagating mode effects seen in a-Si thin films.²¹

III. DISCUSSION

By enforcing the lower-limit of thermal diffusivity, the thermal conductivity of . The importance of this result

While the AF theory is divergent for lattices in the infinite-size limit, the theory provides a plausible lower-limit for a vibrational mode's thermal diffusivity, particularly at high frequencies where the mode lifetime and group velocity (or MFP) cannot be independently defined.^{34,50} This ambiguity can be resolved by considering the thermal diffusivity of a given mode, which incorporates the variation of both group velocity and lifetime (see Section).

Based on the results locating the peaks in the structure factors (Fig.), the reduction

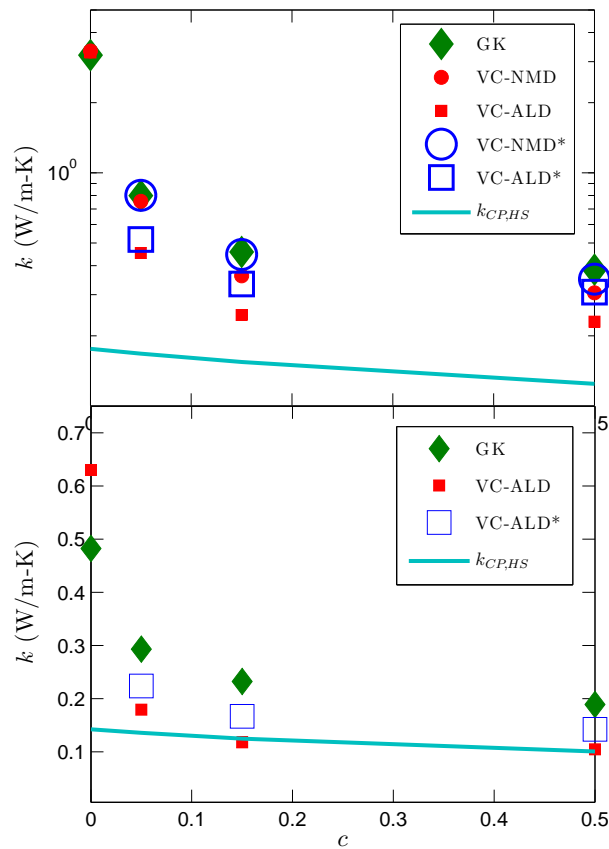


FIG. 10:

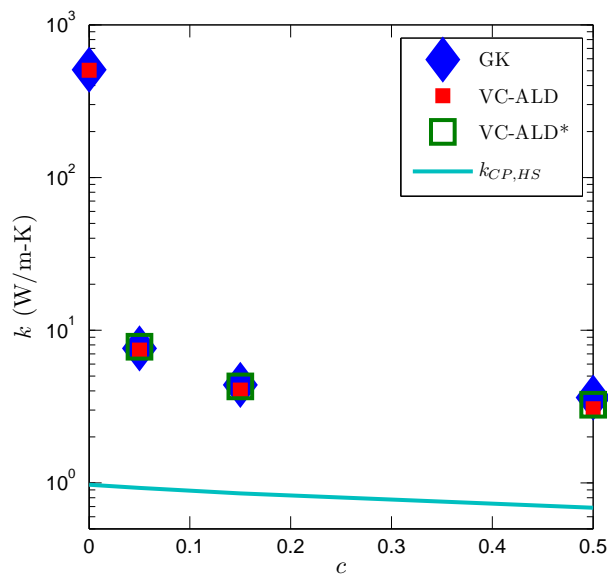


FIG. 11:

due to zone folding would seem to underpredict the group velocity of moderate to high frequency modes.²⁸ Instead, the VC predicted group velocities, when coupled with the VC-NMD predicted mode lifetimes and thermal diffusivity adjusted VC-NMD*, predict thermal conductivities in good agreement with the MD-based GK method.

There is a clear breakdown of the perturbative models used in VC-ALD (Fig. LJ-Diff and Fig. LJ thermal cond 40K), Because of its computational efficiency (Appendix) a simple correction VC-ALD* is useful. This correction brings the predictions for LJ argon into better (though not great) agreement with the MD-based methods, and does not affect the good agreement seen in SW silicon (Fig.).

The existence of a minimum or characteristic mode lifetime for LJ argon (Fig.) is suggested heuristically based on similar limits for electron transport.(cite) Such a minimum, defined in terms of the mode mean free path was, was proposed to explain the plateau temperature dependance of glasses.⁴⁰ There is difficulty in converting between lifetime and mean free path because of the inability to define an effective group velocity for all but the low frequency modes. In this work, the Ioffe-Regel limit ($\tau = 2\pi/\omega$) seems to be a lower limit for the mode lifetimes except for those predicted using VC-ALD (Fig. LJ-Gamma, LJ-Diff and SW-Diff).

For LJ argon, it is possible that the VC group velocities are an over-prediction for modes in a given interval of frequency, but is compensated for by an under-prediction of the lifetimes in the same interval of frequency when compared to the Gamma modes (Fig.). The only constraint we have to compare against is the total vibrational conductivity, which shows good agreement for VC-NMD compared to GK.

Use of the VC approximation is a theoretically and computationally simple way to predict a representative group velocity.

As observed by Kittel, if the sound velocity is used instead of U; and the interatomic spacing is used instead of the mean free path l;, then $tc(T)$ is qual- itatively and semiquantitatively fit at temperatures above the plateau region. In fact, Slack showed that the same model is useful for crystalline insulators with strong scattering.(waiting for ILL).⁵¹

While there is no theoretical justification for the lower limit to the mode mean-free path.⁴⁰ For the lattices studied in this work, the more appropriate quantity to consider is the mode diffusivity since both the effective mode lifetime and group velocity are varying with frequency (Fig.). Since the Allen-Feldman theory does not rely on the assumption

of propagating phonons we expect the results for d to be valid even in the high-frequency regime, where the diffusivity cannot be factorized into a product of $l(\omega)$ times a frequency-independent speed of sound.

In these ordered and disordered lattices, it is difficult to separate the contributions to the total vibrational conductivity from $D_{ph}(\kappa)$ and D_{AF} unless the lower limit $D_{CP,HS}$ or $D_{AF,HS}$ are used.

The theory by Tamura is able to treat disorder scattering in an arbitrary crystal with dispersion. The theory, however, fails to predict the lifetimes of high-frequency modes, which are critical to the total thermal conductivity in LJ argon (see Fig. and). To match the predicted phonon lifetime at high frequency for $c = 0.05$ ($\tau(\kappa) \propto const.$, Fig.), the Tamura theory (to order 2, $g_2(b)$) requires a DOS which scales as $D(\omega(\kappa)) \propto const..$ Clearly from Fig. , this is not the case with either the VC or Gamma modes. To match the predicted phonon lifetime at high frequency for $c = 0.5$ ($\tau(\kappa) \propto 1/\omega(\kappa)$, Fig. , also true for all c in SW silicon), The higher-order terms in the Tamura theory are demonstrated to be large in Fig., but it is unclear if and how they are responsible for the underpredictions of the VC-ALD method for LJ argon.

While Broido found that omission of optical scattering overpredicts the thermal conductivity of bulk Si by a factor of 2-3, optical modes contribute less than 5% to thermal conductivity itself. Similarly, the diffusivity adjusted thermal conductivities of SW Si are increased by less than about 1%, demonstrating the the high frequency and optical modes are also unimportant to thermal transport in Si alloys.

For the perfect system, phonon modes with nearly zero group velocity (optical modes and acoustic modes at the BZ boundaries) have essentially zero thermal diffusivity and contribute nearly nothing to the thermal transport, while the modes themselves are important to the scattering of other phonons.(cite) In the disordered lattices under the AF theory, modes important to thermal transport have a finite thermal diffusivity, as opposed to the minimum $D_{th} \approx 0$ for phonons in a perfect lattice. This finite thermal diffusivity limit is the cause for the large (LJ argon Fig.) and small (SW silicon Fig.) descrepcny between the thermal conductivity prditions of VC-ALD and VC-NMD versus

High thermal conductivity materials tend to have a conductivity spectrum which is peaked in the low frequency range.(cite) It is in this range where the mode lifetimes follow closely the scalings with frequency which can be predicted by the perturbative models for intrinsic

and disorder scattering as (Section Eq.).

In contrast, in LJ argon the high frequency phonon mode properties are critical to the thermal transport.(cite) While the low frequency phonon properties predicted by VC-NMD and VC-ALD agree, it is the failure of the perturbative models at high frequency which causes VC-ALD to underpredict. The failure to account for harmonic disordered scattering due to the AF theory is responsible for causing both VC-NMD and VC-ALD to underpredict versus GK, which affects the high frequency modes significantly. LJ argon, with lower frequencies, lifetimes, and group velocities compared to “stiff” SW silicon, is considered a “soft” system. The predictions using VC-NMD, VC-ALD demonstrate the importance of explicit disorder modeling in “soft” systems and possible underprediction of the thermal properties.¹

For SW silicon, the low frequency modes dominate thermal transport even in the heavily disordered alloy.(cite new Hopkins) It is thus unsurprising that predictions for SW silicon using VC-ALD agree well with VC-NMD and GK. This is also a plausible explanation for the success of predictions using VC-ALD and ab initio calculations compared to experiment for “stiff” systems (i.e. Si-Ge).(cite)

IV. SUMMARY

Results in this work suggest that the lower limit for the mode diffusivity lattices with thermal conductivities which are near the high-scatter limit.

Acknowledgments

This work was supported in part by a grant of computer time from the DOD High Performance Computing Modernization Program at the US Army Engineer Research and Development Center. We thank Jivtesh Garg, Zhiting Tian, Davide Donadio, Asad Hasan and Craig Maloney for helpful discussions.

Appendix A: Computational Cost

The key to incorporating the effects of disorder explicitly are the use of a large disordered supercells (Section). However, the methods used in this work scale differently with the

size of the supercell considered. The calculations in this work are trivially parallelizable except the MD simulations⁵² and the eigenvalue solution of the Dynamical matrix (Section).²⁷ Efficient MD codes scale linearly with the number of atoms in the system N_a , making the GK method an efficient method for predicting thermal conductivity. However, the computational cost of using large supercells for MD simulation, particularly because of the large number of time steps required (on the order of $10^5 - 10^7$ depending on the system, time step used, etc (cite)), prohibit its use with typical ab initio methods such as plane-wave Density Functional Theory.(cite)

Both VC-NMD and VC-ALD require the eigenvalue solution of a Dynamical matrix of size $(3n, 3n)$ for each irreducible wavevector of the system size considered (Section), which is negligible compared to the other caculations required for both of these methods.(cite) The Gamma-NMD (Section) and AF theory (Section) require the eigenvalue solution of a large Dynamical matrix $(3N_a, 3N_a)$, the solution of which scales as $(3N_a)^3$ (Section). The AF theory is limited to small supercells using ab initio calculations, making it difficult to asses finite-size effects (Section).

Using the VC-ALD method, the symmetries of the system can be used to drastically reduce the required computations, permitting its use with ab initio methods.^{7,38,53,54} For VC-ALD, the calculation of the intrinsic phonon lifetimes $\tau_{p-p}(\kappa_\nu)$ scales as n^4 ,³⁸ making calcualtions for large unit cells challenging.(cite) Compared to the calculation of the intrinsic phonon lifetimes, calculation of the defect lifetimes $\tau_d(\kappa_\nu)$ (Eq.) is negligible.

Appendix B: NMD using Non-Exact Normal Modes

The NMD method reuquires the atomic trajectories (positions and velocities) from an MD simulation. The MD simulations are performed using the package LAMMPS.⁵² The lengths of the MD simulations were longer than 10 times the longest phonon lifetime in the system. These can be estimated a priori from the VC-ALD predicted phonon lifetimes. For LJ argon and SW silicon, the simulations were run using time steps of $dt = 0.002$ LJ units and $dt = 0.0005 fs$ for 2^{20} and 2^{22} time steps and the atomic trajectories were sampled every 2^8 and 2^4 time steps, respectively. Ensemble averaging was performed using 10 independent initial randomized velocity distributions.

For a normal mode which is a normal mode of the lattice supercell used for the MD simula-

tions (Section), the autocorrelation of the total and kinetic normal mode energy are damped exponentials with a decay time $\tau(\kappa_\nu)$, the kinetic energy autocorrelation with a cosinusoidal oscillation frequency $2\omega(\kappa_\nu)$.(cite joe) When using the VC normal modes (Section) to map the MD simulation trajectories for the explicitly disordered lattice supercells (Section), the mode total and kinetic energy autocorrelation fucntions do not always follow simple functional forms. This can be illustrated by using spectral-NMD in the frequency domain, where artifacts such as multiple peaks in an isolated mode's energy spectrum (Φ) can be observed (see Fig).(cite) In the case of multiple peaks, the choice of which peak to fit to predict the phonon properties can be ambiguous. However, a lifetime can be predicted unambiguously using Eq. even with these multiple-peak artifacts, particularly because the autocorrelations are damped exponentially. This results is to be expected given that the atomic trajectories contain information about the lattice energy, which from general statistical physics principles will have exponential relaxation behavior in an equilibrium ensemble.^{55–57}

These artifacts are not surprising given two considerations: 1) the MD simulations contain explicit disorder which influences the atomic trajectories 2) the VC normal modes are not the exact normal modes and of the explicitly disordered system. Descrepancies have been observed previously when the exact normal modes of the system are not used.(cite SED) However, the lifetimes predicted using VC-NMD are in fairly good agreement with those calculated using Gamma (Fig.). Several studies have found good agreement for predictions of lifetimes and thermal conductivity using non-exact eigenvector mappings^{8,58} in a wide-range of materials and phonon scattering conditions.^{6,8,58–60} However, it is crucial that results using non-exact mappings are compared to as many alternative methods as possible. In this work, VC-NMD is compared to the other methods Gamma (Section), GK (Section), and VC-ALD (Section). It is important to remember that the VC normal modes are exact in the limit $c \rightarrow 0$. Use of the VC modes at large c pushes the limits of the approximation, but is useful for predicting an effective group velocity (Section) and the predicted lifetimes agree well with those using Gamma (Section).

Appendix C: Calculation of the Gamma Mode Structure Factors

To calculate $S^{L,T}(\omega)$ for a finite-size system, the delta function in Eq. (??) is broadened using a Lorentzian function with a full-width at half maximum $\Gamma_{FMHW} = \delta_{\omega,avg}$, where

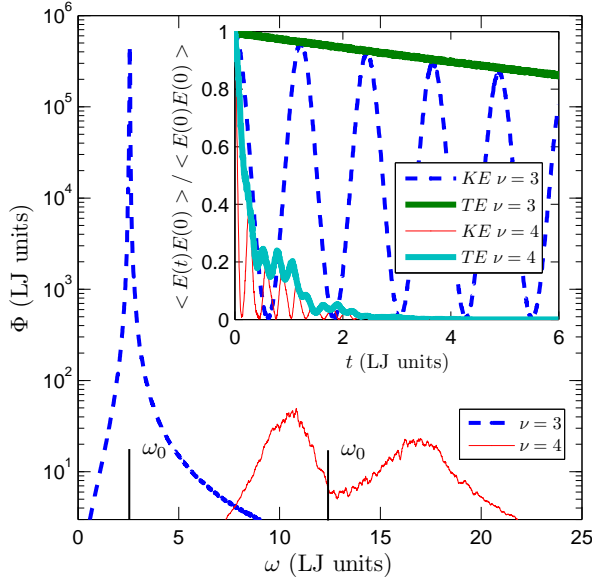


FIG. 12: The spectral energy density Φ of two modes (polarizations $\nu = 3, 4$ at wavevector $[0.2 \ 0 \ 0]$) calculated using VC-NMD for a mass disordered LJ FCC supercell ($N_0 = 8$ and $c = 0.5$, Section). The VC dispersion-predicted peaks are labeled by ω_0 . Inset: the same mode's energy (kinetic (KE) and total (TE)) autocorrelation functions. Note the additional harmonic effects in the KE and TE autocorelation functions for $\nu = 4$ which are due to the double peaks in Φ . A mode lifetime can be extracted unambiguously using the integral of the TE autocorrelation function (Section).

$\delta_{\omega,avg}$ is the average frequency spacing. Allen et al³⁶ demonstrated using a model of a-Si that the structure factor for large wavevector broadens so that the linewidth $\Gamma_{SF} > \omega$.³⁹ For the system sizes studied, Γ_{SF} scale with the broadening factor Γ_{FMHW} for all peaks except those at high frequencies.

For the range of broadening factors considered ($\Gamma_{FMHW} = \delta_{\omega,avg}$ to $50\delta_{\omega,avg}$) the linewidths extracted for all c generally satisfy $\Gamma_{SF} > \omega$. For all broadening factors, the linewidths (inverse lifetimes, $\tau_{SF} = 1/2\Gamma_{SF}$) at high frequency are in better agreement with the lifetimes predicted by VC-NMD rather than VC-ALD, where generally $\tau > 2\pi/\omega$ (Ioffe-Refel limit, Fig.).³⁹ This gives a bit more justification for the use of the VC predicted group velocities both VC-NMD and VC-ALD, even for large wavevector and c .

In general, the polarization of the eigenvectors $e(\kappa_\alpha^b)$ will not be purely transverse or longitudinal along the reciprocal directions. Even for the simple LJ argon system, this can make it difficult to uniquely identify the different polarizations with the various peaks in

the structure factors. For SW silicon, similar good agreement can be seen along the high symmetry directions for the acoustic branches, while the optical modes and more complicated polarizations are too difficult to identify in an automated way. In general, the acoustic branches can be identified, provided they are well separated in energy (or frequency) from any optical branches.^{34,58}

Appendix D: Finite Simulation-Size Scaling for Thermal Conductivity

To predict a bulk thermal conductivity, extrapolation is used by the following finite size scaling $1/k \propto 1/N_0$. For VC-NMD and VC-ALD, the validity of the finite-size scaling requires the low frequency modes in the finite system to be dominated by intrinsic scattering ($\tau(\kappa) \propto \omega(\kappa)^{-2}$, Section) and follow the Debye approximation with respect to $v_{g,n}$ (Section) and DOS $D(\omega(\kappa))$ (Section).^{6,7} For LJ argon, this requirement is satisfied for modest system sizes (for $N_0 = 6$ to 12) so that both VC-NMD and VC-ALD predictions can be extrapolated to a bulk value. For SW silicon, the thermal conductivity is dominated by low-frequency modes (Fig.). Because of this, large system sizes (up to $N_0 = 40$) are needed to satisfy the extrapolation requirements and only VC-ALD can be used.(cite) This demonstrates the computational efficiency of the VC-ALD method which is necessary when computationally expensive ab initio methods are used (Section).^{1,3,4,7}

System sizes of up to $N_0 = 38$ are required to predict converged thermal conductivity of SW silicon alloys. For Si modeled using the Tersoff potential, system sizes of up to 64000 atoms are required to observe converged values of thermal conductivity using the GK method.⁶¹ We find that similar system sizes are also required for

For the GK method, smaller system sizes $N_0 \leq 12$ are used for the finite size extrapolation for LJ argon and SW silicon . The validity of this result can be explained in terms of a combination of effects which are specific to the MD simulations.⁷ In fact, for $c = 0$ the GK results are independent of system size for $N_0 = 4$ to $N_0 = 12$ for LJ argon.

-
- * Electronic address: mcgaughhey@cmu.edu
- ¹ Z. Tian, J. Garg, K. Esfarjani, T. Shiga, J. Shiomi, and G. Chen, Phys. Rev. B **85**, 184303 (2012), URL <http://link.aps.org/doi/10.1103/PhysRevB.85.184303>.
- ² A. Ward and D. A. Broido, Phys. Rev. B **81**, 085205 (2010), URL <http://link.aps.org/doi/10.1103/PhysRevB.81.085205>.
- ³ L. Lindsay, D. A. Broido, and T. L. Reinecke, Phys. Rev. Lett. **109**, 095901 (2012), URL <http://link.aps.org/doi/10.1103/PhysRevLett.109.095901>.
- ⁴ J. Garg, N. Bonini, B. Kozinsky, and N. Marzari, Phys. Rev. Lett. **106**, 045901 (2011), URL <http://link.aps.org/doi/10.1103/PhysRevLett.106.045901>.
- ⁵ T. Shiga, J. Shiomi, J. Ma, O. Delaire, T. Radzynski, A. Lusakowski, K. Esfarjani, and G. Chen, Phys. Rev. B **85**, 155203 (2012), URL <http://link.aps.org/doi/10.1103/PhysRevB.85.155203>.
- ⁶ J. Shiomi, K. Esfarjani, and G. Chen, Physical Review B **84**, 104302 (2011).
- ⁷ K. Esfarjani, G. Chen, and H. T. Stokes, Physical Review B **84**, 085204 (2011).
- ⁸ N. d. Koker, Physical Review Letters **103**, 125902 (2009), URL <http://link.aps.org/abstract/PRL/v103/e125902>.
- ⁹ H. Bao, B. Qiu, Y. Zhang, and X. Ruan, Journal of Quantitative Spectroscopy and Radiative Transfer **113**, 1683 (2012), ISSN 0022-4073, URL <http://www.sciencedirect.com/science/article/pii/S0022407312002336>.
- ¹⁰ B. Abeles, Phys. Rev. **131**, 19061911 (1963), URL <http://link.aps.org/doi/10.1103/PhysRev.131.1906>.
- ¹¹ S.-i. Tamura, Phys. Rev. B **27**, 858866 (1983), URL <http://link.aps.org/doi/10.1103/PhysRevB.27.858>.
- ¹² D. G. Cahill and F. Watanabe, Phys. Rev. B **70**, 235322 (2004), URL <http://link.aps.org/doi/10.1103/PhysRevB.70.235322>.
- ¹³ D. G. Cahill, F. Watanabe, A. Rockett, and C. B. Vining, Phys. Rev. B **71**, 235202 (2005), URL <http://link.aps.org/doi/10.1103/PhysRevB.71.235202>.
- ¹⁴ W. A. Kamitakahara and B. N. Brockhouse, Phys. Rev. B **10**, 12001212 (1974), URL <http://link.aps.org/doi/10.1103/PhysRevB.10.1200>.

- ¹⁵ F. H. Stillinger and T. A. Weber, Physical Review B **31**, 52625271 (1985).
- ¹⁶ P. B. Allen and J. L. Feldman, Physical Review B **48**, 1258112588 (1993).
- ¹⁷ K. Momma and F. Izumi, Journal of Applied Crystallography **41**, 653658 (2008), URL <http://dx.doi.org/10.1107/S0021889808012016>.
- ¹⁸ J. M. Ziman, *Electrons and Phonons* (Oxford, New York, 2001).
- ¹⁹ R. Peierls, *Quantum Theory of Solids* (Oxford University Press, 2001).
- ²⁰ D. A. McQuarrie, *Statistical Mechanics* (University Science Books, Sausalito, 2000).
- ²¹ Y. He, D. Donadio, and G. Galli, Applied Physics Letters **98**, 144101 (2011).
- ²² J. L. Feldman, M. D. Kluge, P. B. Allen, and F. Wooten, Physical Review B **48**, 1258912602 (1993).
- ²³ A. J. H. McGaughey, PhD thesis, University of Michigan, Ann Arbor, MI (2004).
- ²⁴ J. V. Goicochea, M. Madrid, and C. H. Amon, Journal of Heat Transfer **132**, 012401 (2010).
- ²⁵ D. P. Sellan, J. E. Turney, A. J. H. McGaughey, and C. H. Amon, Journal of Applied Physics **108**, 113524 (2010).
- ²⁶ M. T. Dove, *Introduction to Lattice Dynamics* (Cambridge, Cambridge, 1993).
- ²⁷ J. D. Gale and A. L. Rohl, Molecular Simulation **29**, 291 (2003).
- ²⁸ J. C. Duda, T. S. English, D. A. Jordan, P. M. Norris, and W. A. Soffa, Journal of Physics: Condensed Matter **23**, 205401 (2011), URL <http://stacks.iop.org/0953-8984/23/i=20/a=205401>.
- ²⁹ A. M. Bouchard, R. Biswas, W. A. Kamitakahara, G. S. Grest, and C. M. Soukoulis, Phys. Rev. B **38**, 1049910506 (1988), URL <http://link.aps.org/doi/10.1103/PhysRevB.38.10499>.
- ³⁰ A. J. H. McGaughey and M. Kaviany, in *Advances in Heat Transfer, Volume 39*, edited by G. A. Greene, Y. I. Cho, J. P. Hartnett, and A. Bar-Cohen (Elsevier, 2006), p. 169255.
- ³¹ D. Cahill and R. Pohl, Annual Review of Physical Chemistry **39**, 93121 (1988).
- ³² D. Donadio and G. Galli, Phys. Rev. Lett. **102**, 195901 (2009).
- ³³ Y. He, D. Donadio, J.-H. Lee, J. C. Grossman, and G. Galli, ACS Nano **5**, 1839{\backslash}961844 (2011).
- ³⁴ J. L. Feldman, P. B. Allen, and S. R. Bickham, Phys. Rev. B **59**, 35513559 (1999), URL <http://link.aps.org/doi/10.1103/PhysRevB.59.3551>.
- ³⁵ S. Volz and G. Chen, Physical Review B **61**, 26512656 (2000).
- ³⁶ P. B. Allen, J. L. Feldman, J. Fabian, and F. Wooten, Philosophical Magazine B **79**, 1715

(1999).

- ³⁷ A. J. C. Ladd, B. Moran, and W. G. Hoover, Physical Review B **34**, 50585064 (1986).
- ³⁸ J. E. Turney, PhD thesis, Carnegie Mellon University, Pittsburgh, PA (2009).
- ³⁹ S. N. Taraskin and S. R. Elliott, Philosophical Magazine Part B **79**, 17471754 (1999), URL <http://www.tandfonline.com/doi/abs/10.1080/13642819908223057>.
- ⁴⁰ J. E. Graebner, B. Golding, and L. C. Allen, Phys. Rev. B **34**, 56965701 (1986), URL <http://link.aps.org/doi/10.1103/PhysRevB.34.5696>.
- ⁴¹ D. J. Ecsedy and P. G. Klemens, Phys. Rev. B **15**, 59575962 (1977), URL <http://link.aps.org/doi/10.1103/PhysRevB.15.5957>.
- ⁴² P. G. Klemens, Proceedings of the Physical Society. Section A **68** (1955).
- ⁴³ P. G. Klemens, Proceedings of the Physical Society. Section A **70**, 833 (1957), URL <http://stacks.iop.org/0370-1298/70/i=11/a=407>.
- ⁴⁴ A. Skye and P. K. Schelling, Journal of Applied Physics **103**, 113524 (2008), URL <http://link.aip.org/link/?JAP/103/113524/1>.
- ⁴⁵ P. Sheng, *Introduction to Wave Scattering: Localization and Mesoscopic Phenomena* (Springer, 2006), ISBN 9783540291565.
- ⁴⁶ V. Vitelli, N. Xu, M. Wyart, A. J. Liu, and S. R. Nagel, Phys. Rev. E **81**, 021301 (2010), URL <http://link.aps.org/doi/10.1103/PhysRevE.81.021301>.
- ⁴⁷ S. Shenogin, A. Bodapati, P. Kebinski, and A. J. H. McGaughey, Journal of Applied Physics **105**, 034906 (2009), URL <http://link.aip.org/link/?JAP/105/034906/1>.
- ⁴⁸ C. Kittel, Physical Review **75**, 974 (1949).
- ⁴⁹ P. Sheng and M. Zhou, Science **253**, 539542 (1991), URL <http://www.sciencemag.org/content/253/5019/539.abstract>.
- ⁵⁰ N. Xu, V. Vitelli, M. Wyart, A. J. Liu, and S. R. Nagel, Phys. Rev. Lett. **102**, 038001 (2009), URL <http://link.aps.org/doi/10.1103/PhysRevLett.102.038001>.
- ⁵¹ G. A. Slack (Academic Press, 1979), vol. 34 of *Solid State Physics*, pp. 1 – 71, URL <http://www.sciencedirect.com/science/article/pii/S0081194708603598>.
- ⁵² S. Plimpton, Journal of Computational Physics **117**, 1 (1995), ISSN 0021-9991, URL <http://www.sciencedirect.com/science/article/pii/S002199918571039X>.
- ⁵³ K. Esfarjani and H. T. Stokes, Physical Review B **77**, 144112 (2008).
- ⁵⁴ L. Chaput, A. Togo, I. Tanaka, and G. Hug, Phys. Rev. B **84**, 094302 (2011), URL <http://link.aps.org/doi/10.1103/PhysRevB.84.094302>.

- //link.aps.org/doi/10.1103/PhysRevB.84.094302.
- ⁵⁵ G. P. Srivastava, *The Physics of Phonons* (Adam Hilger, Bristol, 1990).
- ⁵⁶ L. Landau, E. Lifshitz, and L. Pitaevskii, *Statistical Physics, Part 2 : Volume 9, Pt 2* (Elsevier Science & Technology Books, 1980), ISBN 9780750626361, URL <http://books.google.com/books?id=NaB7oAkon9MC>.
- ⁵⁷ A. Rajabpour and S. Volz, Journal of Applied Physics **108**, 094324 (2010), URL <http://link.aip.org/link/?JAP/108/094324/1>.
- ⁵⁸ J. A. Thomas, J. E. Turney, R. M. Iutzi, C. H. Amon, and A. J. H. McGaughey, Physical Review B **81**, 081411(R) (2010).
- ⁵⁹ Z.-Y. Ong, E. Pop, and J. Shiomi, Physical Review B **84**, 165418 (2011).
- ⁶⁰ B. Qiu, H. Bao, G. Zhang, Y. Wu, and X. Ruan, Computational Materials Science **53**, 278 (2012), ISSN 0927-0256, URL <http://www.sciencedirect.com/science/article/pii/S0927025611004770>.
- ⁶¹ Y. He, I. Savic, D. Donadio, and G. Galli, Phys. Chem. Chem. Phys. pp. – (2012), URL <http://dx.doi.org/10.1039/C2CP42394D>.